Supplementary Materials for

Genomic determinants of coral heat tolerance across latitudes

Groves B. Dixon, Sarah W. Davies, Galina A. Aglyamova,
Eli Meyer, Line K. Bay,* Mikhail V. Matz*

*Corresponding author. E-mail: l.bay@aims.gov.au (L.K.B.); matz@utexas.edu (M.V.M.)

This PDF file includes:

Materials and Methods
Supplementary Text
Figs. S1 to S8
Table S1
References

Other Supplementary Material for this manuscript includes the following:
(available at www.sciencemag.org/cgi/content/full/348/6242/1460/DC1)

Databases S1 and S2

Materials and Methods

Environmental data

Temperature data for the reef flats of Princess Charlotte Bay location (Wilkie Island) and Orpheus Island (Cattle Bay) were obtained from AIMS temperature logger data archive (www.aims.gov.au). For Cattle Bay the logger was placed in 3.5 m water and monthly averages were based on 17 years of data (1993 – 2010). For Wilkie Island the logger was found in 3.7 m of water and averages were based on 11 years on data (2000 – 2012).

Larval rearing

Coral larval cultures were established and reared as described previously (*15*), with one modification of using less dense cultures (0.5 larvae per mL). Ten crosses were established and reared in triplicate cultures. The two crosses (DA and DB) that are missing from the complete 4x4 diallel design scheme (Fig. 1 B) were not possible to establish due to the limited amount of eggs released by the colony D. At midday on the 5th day 50-70 larvae from each culture (n=30 larval samples) were preserved in 96% ethanol for tag-based RNA-seq.

Scoring larvae for heat tolerance

On the 6th day post fertilization, samples of 20 larvae (6 replicate samples per culture) were placed in netted well plates allowing water and waste exchange with the large volume (60L) of filtered seawater in the water bath. The temperature was ramped from 28 to 35.5^{o}C over 12 hours and the surviving larvae were counted every 4-6 hours over the next 37 hours. No larval mortality was observed in the control experiment set at ambient temperature (28°C). One of the 30 cultures (DA2) was accidentally lost on the 6th day and was not scored for heat tolerance.

Statistical analysis of larval heat tolerance

Heat tolerance of larvae was modeled as odds of survival under heat stress at 27 and 31-hour time points, when the differences in mortality between larval families were the most pronounced (Fig. 2A). To assess the effect of PCB parentage on heat tolerance, an over-dispersed binomial mixed model with fixed factors of timepoint (27 or 31 hours, used as categorical factor levels) and pcb.parent ("none", "dam", "sire", or "both") was fitted to the counts data using the package MCMCglmm in R (*16*). The model also included a scalar random effect of culture to account for repeated measures across timepoints. The p-values for pairwise comparisons between the pcb.parent factor levels were calculated based on samples from posterior distributions of parameter values. To evaluate the proportion of variance explained by genetic factors, another over-dispersed binomial mixed model was constructed in MCMCglmm, with a single fixed effect of timepoint (27 or 31), and sire, dam, and their interaction as random effects; plus a scalar random effect of culture to account for repeated measures. The model used identical weakly informative inverse Wishart priors (V =1, nu=0.1) for all variance components to indicate that some variance was expected for each. The proportions of variance attributable to parental

effects were calculated based on the samples from posterior distributions of the corresponding variance components.

Adult heat stress experiment

Small branches of parental colonies with 3-5 tips each were fragmented from parental colonies and allowed to acclimate in a shaded flow-through outdoor tank at the ambient temperature (28°C) for 5 days. A subset of the fragments was then subjected to heat stress for 3 days (31.5^{o}C, ramped from 28°C over 24 hours). On the morning of the fourth day three fragments from each colony from the control tank and heat-stress tank were sampled for tag-based RNA-seq resulting in n=3 replicates per condition per colony, 24 samples total. Both larval and adult samples were preserved in 96% ethanol and kept at -20°C until processed.

Tag-based RNA-seq

This method is specifically designed to measure abundances of polyadenylated transcripts and is cost-effective due to a streamlined library preparation protocol and efficient use of sequencing for quantification purposes (the method generates a single read per transcript, representing a random fragment near the 3'-end). The method generally follows the protocol described earlier (*8*) but includes modifications in oligonucleotide sequences and bioinformatics pipeline to adapt it for Ilumina HiSeq. One noteworthy modification that we introduce here is removal of PCR duplicates, based on the match of the first 20 bases of read sequence (variable because of the random fragmentation of the original transcript) plus the match of the 64-fold degenerate leader incorporated during cDNA synthesis. The resulting counts, which we term unique transcript counts (UTCs), represent unique observations of independent transcripts for all but the most highly abundant targets. The current version of the library preparation protocol and the bioinformatics pipeline can be downloaded from https://sourceforge.net/projects/tag-based-rnaseq/ .

Larval samples were sequenced at the depth of 1.4-7.1 million 50bp single-end reads per sample, which generated 0.24-1.17 (median: 0.50) million UTCs. Adult samples were sequenced at the depth 1.9-11.6 million reads and generated 0.28-1.52 (median: 0.67) million UTCs per sample. The reads were mapped against *A. millepora de novo* transcriptome (*17*).

Analysis of differential gene expression

The analysis of UTC data was performed using the DESeq package in R. Dispersions were estimated using the model-aware Cox-Reid adjusted maximum likelihood estimator ("pooled-CR" option). For the larvae, dispersions were estimated according to the formula "count~family". The association with heat tolerance was tested using a negative-binomial model with continuous predictor variable "survival", which was the log-odds of each culture's survival under heat stress derived from the genetics model. Differential expression among larval families was detected using a negative-binomial model with "family" as a single factor with 10 levels corresponding to the crosses. The significance of "survival" and "family" predictors for each gene was estimated using a likelihood ratio

test against a null model with no predictor variables. For adults, dispersions were estimated according to the formula "count~individual+treatment+individual:treatment". The significance of each term for each gene was estimated using a series of nested likelihood ratio tests. Transcripts comprising the lower 36% (larvae) or 17% (adults) quantile for mean UTC across samples were excluded from further analysis to maximize the number of differentially expressed genes (DEGs) post false discovery rate correction, following the procedures implemented in genefilter package for R (*18*). All heatmaps were constructed using custom R script uniHeatmap.R (Database S1).

Transcriptome annotation

The Moya et al (*17*) transcriptome was annotated based on two resources: the Joint Genome Institute's annotated proteome of the starlet sea anemone *Nematostella vectensis* and in-depth annotations of the *Acropora digitifera* proteome (*19*). Based on manual verifications of a subset of *A. digitifera* annotations, they were pre-filtered to include protein sequences longer than 60 amino acids with the annotation assigned based on the listed e-value = 1e-20 or better. The GO, KEGG, KOG, and gene name annotations were transferred to an *A.millepora* contig if the contig matched one or both of these two resources with e-value = 1e-5 or better in blastx (*20*). The gene name transferred from the *N. vectensis* resource was in fact a KOG term name. If both resources supplied gene names, they were concatenated in the final annotation. The GO annotations assigned to genes that were denoted FOG - "fuzzy orthologous group" (*10*) - in the *N. vectensis* data were removed, since such genes encode multi-functional protein domains that cannot be unambiguously annotated based on blastx match alone.

Gene ontology analysis

For GO analysis we used the rank-based methodology introduced earlier (*21–23*) that is particularly suitable for non-model organisms. The procedure begins with assembling a custom GO database specific for the particular collection of annotated genes, followed by merging GO categories that share too many genes based on hierarchical clustering with complete linkage method. Following Kosiol et al (*22*), the pairwise distance measure used for clustering is the fraction of shared genes relative to the size of the smaller of the two categories. The resulting clusters are then merged at the adjustable dissimilarity threshold, the default (used here) being 0.25: a group of GO categories is merged if the most dissimilar two of them share 75% or more genes. Although it is a very conservative clustering scheme resulting in merging of only very similar categories, it helps reduce the total number of tested GO terms by 30-50% and thus boost the power of the method post correction for multiple comparisons. For each remaining GO category, a delta-rank value is computed based on gene expression measures as the difference between the mean rank of all genes within the GO category and the mean rank of all other genes. This value can be understood as a degree of enrichment of the GO category by up- or down-regulated genes, relative to the rest of the dataset. The significance of this enrichment is calculated using a two-sided Mann-Whitney U-test followed by the false discovery rate correction. The results are plotted as a dendrogram tracing the level of gene sharing between significant categories, indicating the direction of change by text color and significance of change by font type. The major advantage of this approach is that it does not require an

arbitrary discrimination between "significant" and "non-significant" genes. Still, the method also lists the fraction of genes passing a user-defined "good candidate" cutoff relative to the total number of genes annotated with the GO term. These "Fisher-like" numbers are not used for statistical analysis and only serve for illustrative purposes. Note that occasionally a GO term might become significant by MWU test while demonstrating unimpressive Fisher-like numbers, for example, 2/27: it implies that nearly all of the 27 genes belonging to the GO category exhibit a consistent change in the same direction, although only two of them would have passed a formal "significance cutoff". This does not happen too often, though, as can be seen from our figures 3 and S5. The measures of differential expression used here were "signed log-p-values": the negative logarithm of the gene's p-value multiplied by -1 if the gene was down-regulated. Thus, highly significant genes were assigned a larger value on the absolute scale, which was positive if the gene was up-regulated and negative if it was down-regulated. The current version of the methodology implemented using R and perl can be downloaded from https://sourceforge.net/projects/go-mwu/.

KOG class analysis

This analysis follows the same idea as the GO analysis described above, but is based on KOG (clusters of euKaryotic Orthologous Genes) class assignments rather than GO annotations. In contrast to GO annotations, there are only 23 informative KOG classes, which are not hierarchical and have very little or no overlap in genes, which makes it possible to generate compact functional summaries on a whole-transcriptome scale and compare results quantitatively among datasets. The "signed log-p-values", calculated as described in the previous section, were used as measures of differential expression for the new larval and adult datasets. For the previously published larval datasets, which involved minimal replication and thus provided less statistical power, the DESeq-derived log-fold-changes were used. Enrichment of each KOG class with up- or down-regulated genes was inferred based on the class' delta-rank and two-sided Mann-Whitney U test, as described in the previous section. The methodology has been implemented in the R package KOGMWU, which is hosted on the Comprehensive R Archive Network (CRAN) servers.

Heat selection experiment

Aliquots of two replicate cultures of each of the two reciprocal crosses (CA and AC), containing about 1,000 larvae in 2L of filtered seawater, were subjected to the same temperature treatment as during larval heat tolerance profiling (35.5^{o}C, ramped from 28°C over 12 hours). The treatment continued for approximately 36 hours until 30-50 surviving larvae remained in each of the cultures, which were collected for individual genotyping. As a control, 50 larvae were sampled from portions of the same larval cultures that did not undergo heat treatment. The resulting samples comprised 8 separate groups corresponding to 2 reciprocal crosses, 2 larval cultures per cross, and 2 treatments (heat-selected and control) for each culture, 30-50 larvae per treatment.

2bRAD genotyping

2bRAD is a whole-genome genotyping methodology that relies on restriction endonucleases to target the genotyping effort to a small fraction (about 1-5%) of the genome (*12*). Larval and adult coral DNA was isolated using a phenol-chloroform protocol (*24*). A BcgI restriction enzyme was used to generate fragments for sequencing. Sequencing of RAD fragments was performed on an Illumina HiSeq 2500 instrument and generated a total of 224,591,655 raw sequence reads. Reads were 'demultiplexed' based on barcodes incorporated during the ligation and PCR amplification stages. Dual adapters used for demultiplexing reads from offspring were trimmed using a custom perl script. All reads were quality filtered using Fastx Toolkit (http://hannonlab.cshl.edu/fastx_toolkit/). After trimming and quality filtering a total of 180,957,303 reads had been generated from 361 libraries, with an mean count of 501,267 reads ± 39,502 SE. 23 offspring libraries had read counts < 75,000 and were removed from further analysis. The two parental individuals along with two additional adult samples were sequenced in triplicate and with greater read depth. Mean read counts for these 12 samples was 3,759,904 ± 478,584 SE. Mean depth for the offspring samples was 413,525 ± 18,895 SE. Of the 326 offspring samples included in the analysis, 190 were control samples and 136 were heat selected. The detailed wet lab protocol, bioinformatic pipeline and custom scripts for performing 2bRAD analysis are provided as supplementary file 6. The current version of the methodology, including a novel modification allowing for removal of PCR duplicates, can be downloaded from https://sourceforge.net/projects/gatk-2brad/ .

Variant calling

Variant discovery, genotyping and filtering was performed using The Genome Analysis Tookit version 3.1-1 (GATK) (*25*). The basic pipeline framework includes mapping, realigning the reads around indels, recalibrating base quality scores, calling putative variants, then developing an adaptive filtering model to select highly confident variants (*26*). Descriptions of the tools, usage, and best practices can be found on the GATK website (https://www.broadinstitute.org/gatk/). The following is a description of our adaptation of this framework.

Reads were mapped using Bowtie2 (*27*) with the –local option against a draft assembly of the *A. millepora* genome released to the public by David Miller and coworkers (James Cook University) in July 2011 under an 18-month embargo. The alignment files generated from Bowtie2 were used as input for the GATK variant calling pipeline. Following realignment around indels, a first round of putative variants was generated using GATK's UnifiedGenotyper. From these initial variants calls, the top 10th percentile for quality was selected using a custom python script. These high confidence base calls were passed as the 'knownSites' to GATK's BaseRecalibrator, which recalibrates base quality scores to remove biases of particular sequencing technologies and contexts (*26*). The realigned and recalibrated reads were then used to generate a second set of putative variants.

The next step is the variant recalibration step, which provides estimates of the probability that each putative variant is an actual SNP. These estimates are used to filter the putative

variants to minimize false discoveries. The VariantRecalibrator program generates an adaptive error model based on a set of user supplied set of "true" SNPs and a chosen set of VCF annotations such as read depth or inbreeding coefficient (*26*). The source of the "true" SNPs supplied to the VariantRecalibrator should be one that is well established for the particular organism. Lacking an established set of SNPs for *A. millepora*, we used the variants that were reproducibly genotyped across the technical replicates of our four parental colonies instead (3 replicates x 4 colonies = 12 genotyping sets). For a locus to be considered a "true variant" for the recalibration procedure, out of 12 genotyping sets not more than three (25%) could be missing data for the locus, and all the non-missing calls should agree among replicates. The result was 9,338 variant sites (out of 68,141) that were both polymorphic among the adults and had fully consistent genotype calls between technical replicates. This set was used as the 'true' sites for the variant recalibration. The statistics used to build the error model in our case were total unfiltered depth of coverage (DP), inbreeding coefficient (InbreedingCoeff), quality by depth (QD), and the root mean square of the mapping quality of the reads across all samples (MQ). The filtering process represents a compromise between maximizing sensitivity for recognizing the "true" variants and minimizing false discoveries. To facilitate filtering, the VariantRecalibrator generates tranches of the variant calls with varying truth sensitivities (the percentage of "true" variants captured in the tranche). The false discovery rate for each tranche is estimated based on the difference between an expected transition/transversion (Ti/Tv) ratio and the Ti/Tv ratio for the variants included in the tranche. Tranches with Ti/Tv ratio lower than the expected value are inferred to include false positives. The target Ti/Tv value in *A. millepora* was 1.41, estimated from the same 9,338 reproducibly genotyped SNPs that were used to build the error model. In applying the recalibration we chose the tranche with 96% truth sensitivity, which had a Ti/Tv ratio of ~1.43. The final output of the genotyping pipeline was a set of 55,211 filter passing variants recorded in VCF format.

Selection of variants for mapping

The following is a description of additional filters used to prepare the genotype data for linkage mapping. These filters were applied using custom python scripts and are described in order of their implementation. Using vcftools (*28*) individual genotype calls with a sample depth of less than 6 reads were changed to missing data, to reduce the incidence of false homozygotes. Assuming equal probabilities of sequencing the paternal and maternal chromosome at a given site, the probability of not encountering a second allele (potentially leading to a false homozygote call) can be described as $2^{-(n-1)}$, where n is the depth of coverage for the individual at that site. We chose a depth threshold of six, with an estimated probability of missing a second allele of 1/32 as a comfortable compromise between excluding too many genotype calls and having too little confidence in homozygote calls. We next filtered for variant quality based on agreement between technical replicates. Variants that had missing data for two of the three replicates for either parent were removed (27859 variants) as well as variants with more than one disagreement between parent replicates (544 variants). In cases of a single disagreement between replicates the most common genotype was retained as the consensus type for that parent. Variants for which the consensus genotypes for both parents were homozygous were then removed because they were not informative for linkage analysis

using the outbred F1 design (13735 variants). Next we filtered the remaining genotype calls that were incompatible with the parental genotypes. First genotypes with alleles not present in the parental genotypes for that locus (1223 total) were assumed to be sequencing errors and changed to missing data. In addition, a small proportion (2.8%) of the filter-passing genotypes calls were incompatible based on their combinations of parental alleles. A large proportion of these (86%, or 2.4% of all calls) could be inferred as false homozygotes. For instance, in a cross represented by AAxAT, an offspring genotype call of TT should not occur, and is strongly indicative of a false homozygote from a failure to sequence the second allele. Such genotypes were changed to the inferred heterozygote (in the example above, TT genotype call would be changed to AT). The remaining 0.4% of incompatible genotypes could not be resolved and were changed to missing data. Variants genotyped in less than 100 offspring were removed (8174 variants). Filtering for deviation from Mendelian expectations was performed using chi square tests with a threshold of $P = 0.05$. Because we wanted our map to include markers displaying segregation distortion due to heat selection, the Mendelian filtering was performed based only on control samples. As a result 1854 variants showing significant distortion among the controls were excluded, while variants showing distortion specifically among the heat selected samples were retained. The input for linkage analysis contained a total of 3047 passing variants.

Linkage mapping

Linkage analysis was carried out using JoinMap 4.1 (*29*). Markers were categorized by cross types using the annotations given for the outbreeder full sib family protocol in the JoinMap user manual (*30*). Offspring from both reciprocal crosses were used for the analysis and all markers were coded as if parent A was the female and parent C was the male. Initial grouping was carried out using the independence log-odds (LOD) score. A grouping threshold of 12 produced 14 linkage groups corresponding to the haploid number of chromosomes for *A. millepora* (*31*). The independence LOD is based on the G^2 statistic for independence and is not affected by segregation distortion (*30*). After initial groups were established, ungrouped markers were incrementally added to their best fitting linkage groups by walking from an LOD threshold of 11 down to 6.

Ordering of loci was performed using the regression mapping algorithm. This algorithm orders the loci by adding them one at a time to their best fitting positions starting with the most informative markers (*29*). To avoid locally optimal orders, the ripple function was applied after adding each locus. The Kosambi mapping function was used to convert the recombination frequencies into map distances (centiMorgans).

Genomic regions responding to heat selection

By treating a subset of our larval cultures with heat we intended to select for alleles that conferred increased larval tolerance to critically elevated temperatures. If such selection occurred, we would expect to see 1) reproducible differences in allele frequencies between heat selected and control cultures and 2) spatial autocorrelation between RAD loci and the magnitude of selection signal. The second prediction should result from linkage between RAD loci and any alleles that were under selection due to heat

treatment. For the first prediction, we first used Fisher's exact tests (*32*) to compare allele counts between each replicate pair of control and heat treated cultures. *p*-values from replicates were then combined using Fisher's Combined Probability method (*33*). When using this method, it is important to use one-tailed *p*-values so that information on the direction of effect is retained (*34*). This required that we use one-tailed tests for comparisons of allele frequency. To obtain the predicted direction of selection (either for or against the reference allele) at each locus, we calculated the average difference in reference allele frequency for the two replicates for each cross. The sign of the average was used to designate the alternative hypothesis for one-tailed Fisher's exact tests. To compensate for this *post hoc* use of the data to inform one-tailed tests, we multiplied the *p*-values by 2. Combined *p*-values were adjusted to control for false discovery rate (*35*). The genotype calls used to perform all selection analyses were generated using the same filtering parameters described above, with the exception of a read depth threshold of four rather than six was used to change genotypes to missing data.

To visualize genomic regions showing signatures of selection Manhattan plots were generated for each genetic cross by –log transforming the combined *p*-values and plotting them against their predicted chromosomal locations. To test for spatial autocorrelation of the selection signal we used a bootstrap approach. First a null distribution was generated from 10^5 permutations of randomly selecting 15 markers (without replacement) from the dataset and counting the number with Fisher's combined *p*-values less than 0.05. Then each linkage group was divided into equal non-overlapping windows each comprising 15 adjacent RAD loci. For each window, the number of loci with combined *p*-values below 0.05 was counted and compared with the null distribution to provide a bootstrap *p*-value for that window. Following false discovery rate adjustment, window *p*-values less than 0.1 and 0.05 were indicated on the Manhattan plot for each cross. This analysis served to identify additional genomic regions with moderate, but strongly autocorrelated deviations in allele frequency.

Strength of selection

Since in nearly all cases the parental genotypes were of the type AA:Aa, the selection process in the F1 can be viewed as a result of competition between AA homozygote and Aa heterozygote. In such case we calculated selection coefficients using the following equation (*36*):

against the top hit. Alignment coordinates for each contig were recorded as the minimum and maximum alignment positions. When calculating physical distances between genes and RAD loci we used the midpoint of contig's alignment coordinates. We report genes found within 100 kb to either side of the top-scoring RAD locus within the boundaries of the peak.

Supplementary Text

Specific genes associated with larval thermal tolerance

Among the top 5% of the most significantly tolerance-associated annotated genes (Fig. S1, overleaf), there were two proteins with well-known regulatory functions, both up-regulated in heat tolerant larvae: fructose-1,6-bisphosphatase, the key regulatory enzyme in gluconeogenesis (*37*), and aconitase, which down-regulates mitochondrial metabolism under hyperoxic conditions (*38*) and modulates production of iron-binding proteins (*39*). Up-regulation of these genes could indicate healthier metabolic state and heightened capacity to respond to oxidative stress. Tolerance-associated genes also included seven members of the tumor necrosis factor receptor-associated factors (TRAFs), five of which were up-regulated in the tolerant larvae and two of which were down-regulated (Fig. S2, overleaf). TRAFs are important regulators of cell death and cellular responses to stress that have previously been implicated in coral stress response (*9*). It should be noted that the TRAF family appears to have undergone an expansion in acorporid corals: compared to only six TRAF genes in a human, 31 TRAFs were identified in the genome of *Acropora digitifera* (*40*), and we have detected as many as 54 TRAF-related contigs in the *A. millepora* transcriptome (*17*). Another notable multigene family represented among tolerance-associated genes was ATP-gated ion channels (P2X receptors), three of which were up-regulated in tolerant larvae (Fig. S2). The products of these genes are the key components of the purinergic signaling pathway that regulates a variety of whole-organism functions including ciliary beating, extracellular matrix formation, and immunity (*41*) . Finding three out of seven P2X genes present in the transcriptome is unlikely to happen by chance ($P_{\text{Fisher's exact}} = 0.003$), suggesting a previously unrecognized role of purinergic signaling in modulating coral stress physiology. Purinergic signaling pathway also involves nucleoside-triphosphate pyrophosphatases, one of which was up-regulated in tolerant larvae (Fig. S2).

Network analysis of larval gene expression

To examine correlation structure in the larval gene expression data in more detail, we subjected 12,575 genes that tended to be differentially expressed either with respect to larval family or heat tolerance (unadjusted p-value <0.1) to the weighted gene correlation network analysis (WGCNA, *[32]*). This unsupervised methodology is designed to identify groups of genes, termed "modules" (Fig. S6 A), that are co-regulated across samples. The expression of these modules represented by the module's eigengene can then be correlated *post hoc* with other characteristics of the samples ("traits"). We looked for correlations with the identity of the dam to identify modules capturing maternal effects on gene expression, for correlations with specific parents and for correlation with

the number of PCB colonies among parents (0, 1, or 2). Additionally, the "tolerance" trait was specified as the odds survival under heat stress, as inferred by the genetic model.

If the large maternal effect on larval heat tolerance (Fig. 2B) was due to genome-wide maternally transmitted epigenetic modification, one would expect to find pervasive maternal effects on gene expression as well. Of the nineteen identified modules (Fig. S6 A), two were identified as dam-specific since they demonstrated top correlation with dam identity: the "darkgrey" module strongly correlated with dam B (Pearson's $r = 0.89$) and the "blue" module correlated less strongly with dam C ($r = 0.67$, Fig. S5 B). Interestingly, the damC-specific module was the second-largest (1985 genes), the damB-specific module was the smallest (62 genes) and damA-specific module was entirely missing. (Since colony D was crossed with only one other colony as a dam it was not possible to isolate D's dam effect). Such unevenness would be surprising if these effects were due to genome-wide epigenetic modifications, which are presumably present in all adult individuals.

Although the eigengenes of both dam-specific modules were significantly correlated with heat tolerance ($r = 0.55$ in both cases), the strongest relationship with tolerance ($r = 0.7$) was observed for the "greenyellow" module (325 genes, Fig. S6 B). This module also scored the highest in the second metric of module-trait association provided in the WGCNA methodology: the correlation between each gene's module membership score and its significance for the trait (Fig. S6 C). The dam-specific modules demonstrated substantially weaker correlations between module membership and gene significance for tolerance (Fig. S5 D, E). Notably, the "greenyellow" module was also extremely strongly correlated ($r = 0.98$) with the number of PCB parents in the cross ("PCB2" trait on Fig. S6 B), which corresponds well with the observation that higher heat tolerance is contributed by both PCB parents (Fig. 2 C).

While maternal effects varied greatly among parental colonies and demonstrated eigengene-dam correlation of 0.67-0.89, the genetic effects were much more consistent as well as more strongly pronounced. They were represented by four parent-specific modules, one for each parent, comprising 487-700 genes each ("red", "green", "black" and "magenta", Fig. S6 B). These modules were nearly perfectly correlated ($r = 0.99$) with the presence of a particular adult among parents of the larval family, irrespective of whether it was used as a dam or as a sire (Fig. S6 F). Strikingly, the expression of the genes comprising these modules appeared to be directly transmitted from the corresponding parental colonies (Fig. S6 G), indicating additive or dominant inheritance. The notable excess of colony-specific up-regulations in all four parents might reflect their prevalence among dominant effects. The "greenyellow" module shows the most difference between "purebred" OI and PCB families and intermediate expression in mixed-origin families (Fig. S6 F). In adults, the genes from this module were differentially expressed between OI and PCB corals (Fig. S6 G). The "greenyellow" module therefore demonstrates additive mode of expression inheritance. Overall, parent-specific modules and the "greenyellow" module accounted for 2,756 genes with additive or dominant inheritance of expression variation.

Figure S1. **Heat map of the annotated genes within the top 5% (by FDR-adjusted p-value) of the tolerance-associated gene**s. Rows are genes clustered according to correlation of expression across samples (columns, sorted from lowest to highest heat tolerance). The color scale corresponds to $\log_2$ of fold change relative to the gene's mean across samples. The columns (larval cultures) are ordered according to increasing survival under heat stress.

Figure S2. **Heat maps of selected genes and gene families.** The rows are genes, columns are samples arranged in the order of increasing heat tolerance.
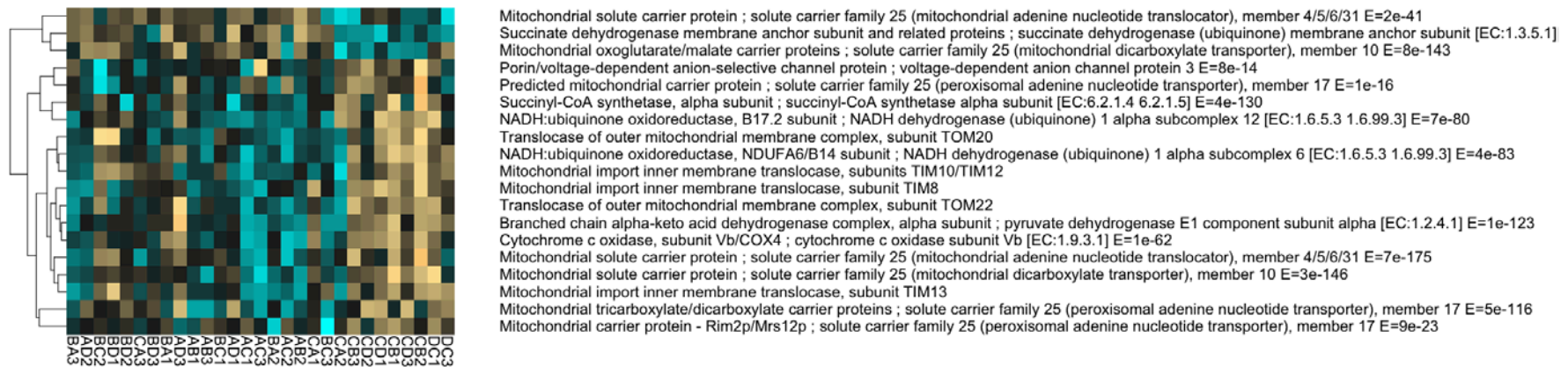
The rows are labeled:

Mitochondrial solute carrier protein ; solute carrier family 25 (mitochondrial adenine nucleotide translocator), member 4/5/6/31 E=2e-41
Succinate dehydrogenase membrane anchor subunit and related proteins ; succinate dehydrogenase (ubiquinone) membrane anchor subunit [EC:1.3.5.1]
Mitochondrial oxoglutarate/malate carrier proteins ; solute carrier family 25 (mitochondrial dicarboxylate transporter), member 10 E=8e-143
Porin/voltage-dependent anion-selective channel protein ; voltage-dependent anion channel protein 3 E=8e-14
Predicted mitochondrial carrier protein ; solute carrier family 25 (peroxisomal adenine nucleotide transporter), member 17 E=1e-16
Succinyl-CoA synthetase, alpha subunit ; succinyl-CoA synthetase alpha subunit [EC:6.2.1.4 6.2.1.5] E=4e-130
NADH:ubiquinone oxidoreductase, B17.2 subunit ; NADH dehydrogenase (ubiquinone) 1 alpha subcomplex 12 [EC:1.6.5.3 1.6.99.3] E=7e-80
Translocase of outer mitochondrial membrane complex, subunit TOM20
NADH:ubiquinone oxidoreductase, NDUFA6/B14 subunit ; NADH dehydrogenase (ubiquinone) 1 alpha subcomplex 6 [EC:1.6.5.3 1.6.99.3] E=4e-83
Mitochondrial import inner membrane translocase, subunits TIM10/TIM12
Mitochondrial import inner membrane translocase, subunit TIM8
Translocase of outer mitochondrial membrane complex, subunit TOM22
Branched chain alpha-keto acid dehydrogenase complex, alpha subunit ; pyruvate dehydrogenase E1 component subunit alpha [EC:1.2.4.1] E=1e-123
Cytochrome c oxidase, subunit Vb/COX4 ; cytochrome c oxidase subunit Vb [EC:1.9.3.1] E=1e-62
Mitochondrial solute carrier protein ; solute carrier family 25 (mitochondrial adenine nucleotide translocator), member 4/5/6/31 E=7e-175
Mitochondrial solute carrier protein ; solute carrier family 25 (mitochondrial dicarboxylate transporter), member 10 E=3e-146
Mitochondrial import inner membrane translocase, subunit TIM13
Mitochondrial tricarboxylate/dicarboxylate carrier proteins ; solute carrier family 25 (peroxisomal adenine nucleotide transporter), member 17 E=5e-116
Mitochondrial carrier protein - Rim2p/Mrs12p ; solute carrier family 25 (peroxisomal adenine nucleotide transporter), member 17 E=9e-23

Figure S3. **Heatmap of genes associated with larval heat tolerance the products of which localize to mitochondria.** These are the genes annotated with Cellular Component GO terms containing the pattern "mitochondr" and passing 10% FDR cutoff for association with larval heat tolerance. The columns (larval cultures) are ordered according to increasing survival under heat stress. Note numerous nuclear-encoded mitochondrial membrane components positively associated with heat tolerance.
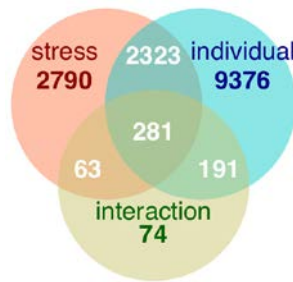
Figure S4. **Venn diagram of genes differentially expressed in adults** (FDR=0.05), with respect to individual, in response to 3-day heat stress (with individual as a covariate), and interaction of these factors.
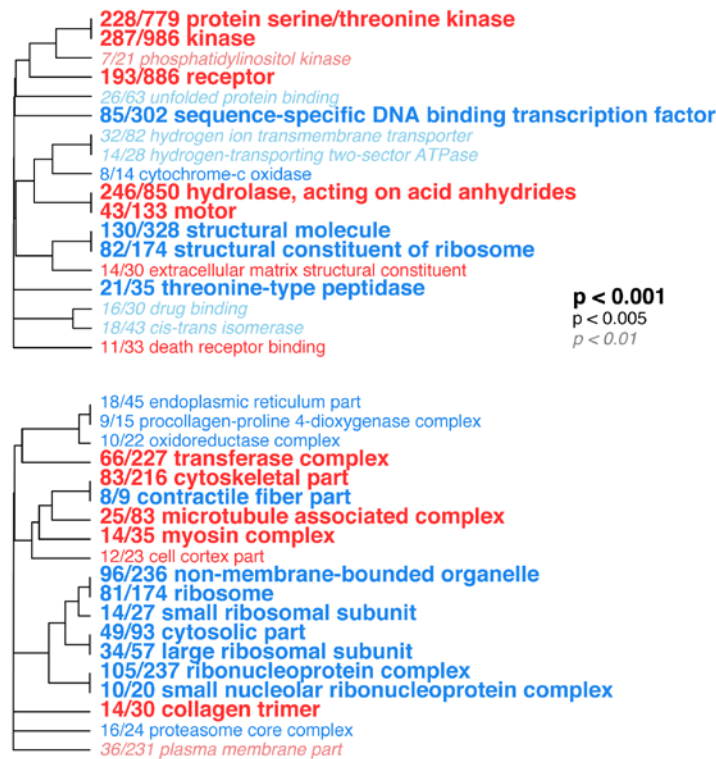

Figure S5. **Gene Ontology categories significantly enriched with genes either positively (red) or negatively (blue) regulated in response to heat stress in adult corals**. Top panel - molecular function, bottom panel – cellular component. The font identifies the FDR-adjusted p-value derived from Mann-Whitney U test. The dendrogram depict the sharing of genes between categories; the categories with no branch length between them are subsets of each other. The fractions correspond to the number of genes with an unadjusted p<0.05 relative to the total number of genes within the category.
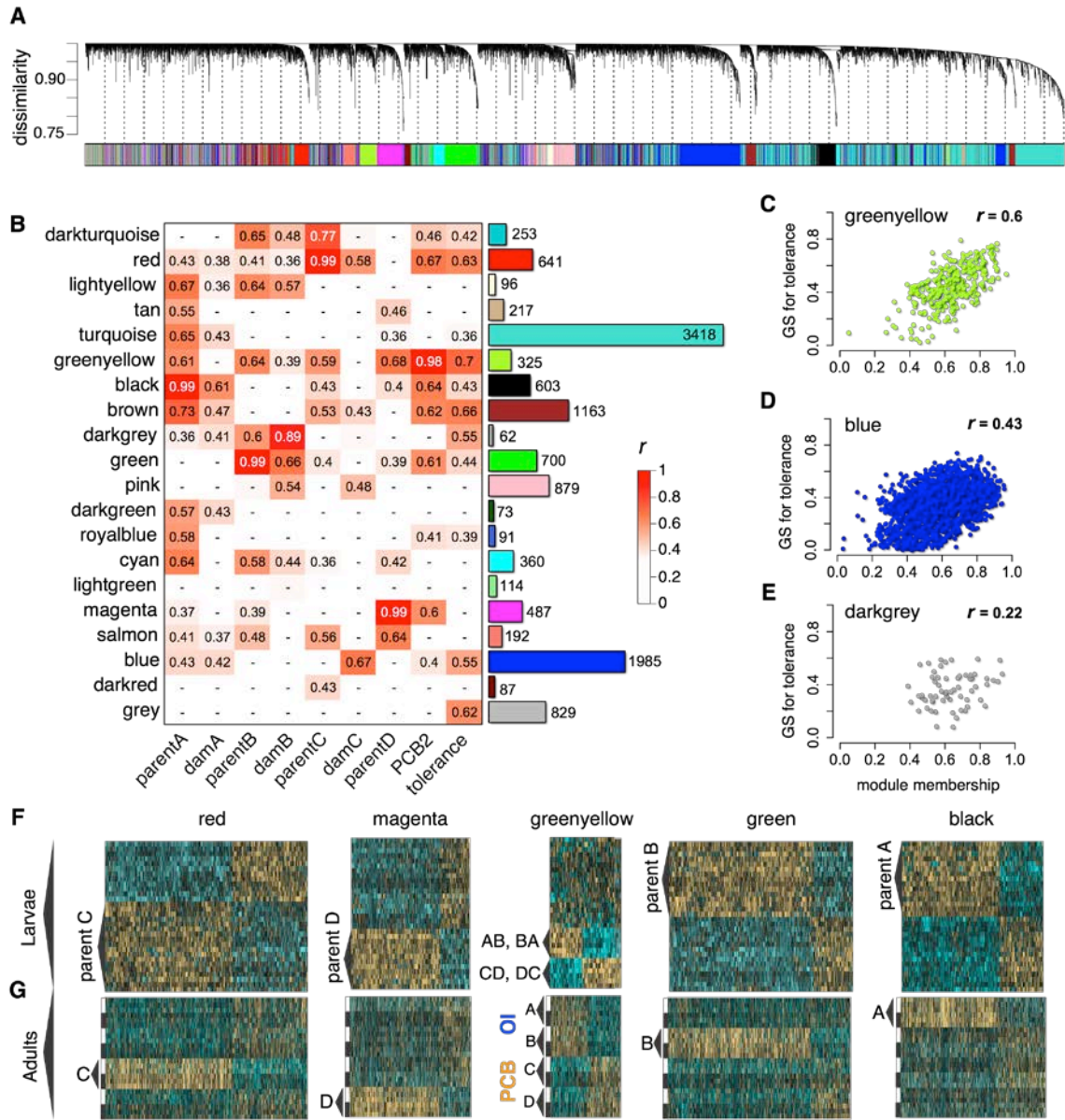
Figure S6. **Network analysis of larval gene expression.** (**A**) The dendrogram showing clustering of genes based on similarity of their expression patterns among larval cultures. The colored bar below the dendrogram denotes inferred co-expression modules. (**B**) Correlations between module eigengenes (rows) and traits (columns): presence-absence of a particular parent ("parentA" to "parentD"), identity of the dam ("damA" to "damC"), number of parents from PCB location ("PCB2") and survival rate under heat stress ("tolerance"). The bar graph and numbers on the right show the number of genes in each module. The numbers in the cells are Pearson's correlation coefficients (not listed for cells with $P_{cor.test} > 0.05$). (**C-E**) Scatterplots illustrating the relationships between a gene's module membership score (X-axis) and the gene's significance (GS) for the tolerance trait (Y-axis). Higher correlation between these measures indicate stronger

association of the module with the trait. Panel C shows the "greenyellow" module that exhibits the strongest association with tolerance according to this metric (as well as according to eigengene-trait correlation on panel B). Panels D and E show the two dam-specific modules capturing maternal effects. (**F**) Heat maps of the larval modules highly correlated with specific parents. Columns are genes and rows are larval cultures. The order of rows on panel F differs among modules, so all cultures sharing a particular parent, irrespective of whether it was used as a dam or as a sire, can be grouped together (C: n=18, D: n=12, A and B: n=15). Note the additive biparental inheritance of the "greenyellow" module. (**G**) Expression of the same genes in the parental adult colonies. Columns are genes in the same order as on panel F, rows marked by white bars are control fragments (n=3 per colony), rows marked by black bars are heat-stressed fragments (n=3 per colony). On panel G, the order of rows is the same across modules.
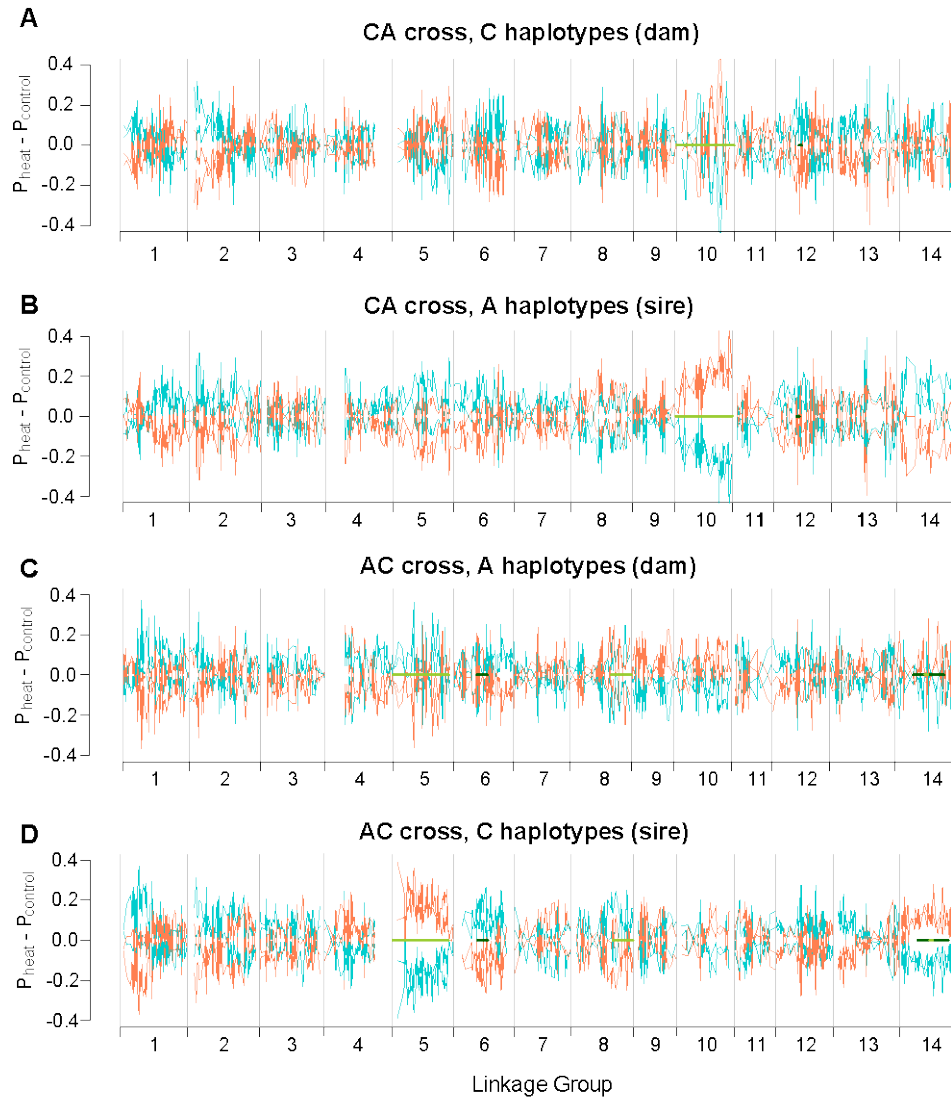
Figure S7. **Allele frequency changes in larval cultures as a result of heat selection**. In each panel, the X-axis gives position of markers in the linkage map and the Y-axis is allele frequency change in selected cultures compared to unselected controls. Panels (A) and (C) show the change in frequencies of maternally-derived variants (i.e., SNPs that were heterozygous in the dam), panels (B) and (D) - the change in frequencies of paternally-derived variants. The two lines of the same color on each panel represent two replicates of the heat stress experiment within each cross; red and blue lines correspond to different haplotypes in the dam (A, C) or sire (B, D). The haplotype color is consistent among the crosses, that is, a blue paternal haplotype in the AC cross is the same as the blue maternal haplotype in the CA cross. The green bars identify regions that show bootstrap-supported significant clustering of low p-values (obtained by Fisher's exact test for each replicate followed by Fisher's combined probability test; light green – 5% FDR, dark green – 10% FDR).

genes in 100kb vicinity of CA-LG10 peak
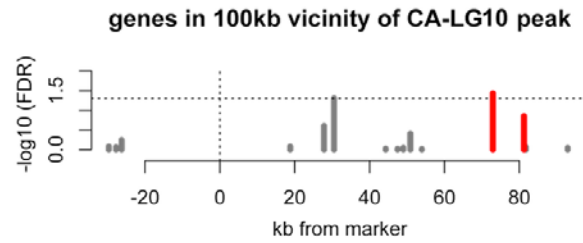
Figure S8. **Expression of genes located within 100 kb of the top-scoring marker within the LG12 in cross CA**. The X-axis is distance from the marker in kilobases, the Y-axis is the $-\log_{10}$ of the false discovery rate-corrected p-value for tolerance-associated expression. Red color marks mitochondrial proteins (both are predicted mitochondrial transporters). The horizontal dashed line corresponds to 5% FDR, the vertical dashed line identifies the position of the top-scoring marker.

Table S1. **Summary of genes located in the 100 kb vicinity of the top-scoring LG10 marker.**

isogroup	Start[1]	End[1]	FDR[2]	Annotation[3]
20639	-29.39	-29.93	0.84	Arginine-rich protein
34591	-27.96	-27.52	0.87	NA
37459	-27.53	-27.14	NA	NA
341	-25.45	-27.04	0.58	voltage-dependent calcium channel N type alpha-1B
19752	-15.64	-14.53	NA	Voltage-gated Ca2+ channel, alpha1 subunit
3507	19.70	17.92	0.83	Histone H3 (Lys9) methyltransferase
24367	27.99	27.68	0.25	Subunit of the major N alpha-acetyltransferase
38063	30.56	30.42	* 0.05	NA
5702	45.02	43.62	0.95	Ca2+/calmodulin-dependent protein kinase
27643	47.73	47.19	0.96	Dynein-associated protein Roadblock
32000	48.86	49.19	0.90	NA
41790	50.71	51.06	0.39	NA
27054	54.08	53.87	0.97	NA
38158	54.39	54.62	NA	NA
17880	72.82	73.04	* 0.037	Predicted mitochondrial carrier protein
18244	81.49	80.99	0.14	Mitochondrial phosphate carrier protein
43758	81.62	81.87	0.87	NA
31960	92.33	92.06	NA	NA
19682	93.49	92.38	0.91	FOG: Zn-finger

1: start and end of the blastn match to the scaffold containing the marker, relative to the marker position (in kilobases).
2: FDR-corrected p-value for the association of the gene with larval heat tolerance. NA means that the expression of this gene was not quantified.
3: Gene annotation. NA means the gene was not annotated in *Nematostella vectensis* and *Acropora digitifera* proteomes.

Database S1: Amillepora_transcriptome_extendedAnnotations.zip (separate file)

This archive contains the reference transcriptome used in this paper, which is an augmented version of Moya et al transcriptome *(17)*.

Database S2: ScriptsAndData.zip (separate file)

This archive contains all the data files and scripts necessary to replicate the analyses.

References

1. T. P. Hughes, A. H. Baird, D. R. Bellwood, M. Card, S. R. Connolly, C. Folke, R. Grosberg, O. Hoegh-Guldberg, J. B. Jackson, J. Kleypas, J. M. Lough, P. Marshall, M. Nyström, S. R. Palumbi, J. M. Pandolfi, B. Rosen, J. Roughgarden, Climate change, human impacts, and the resilience of coral reefs. *Science* **301**, 929–933 (2003). Medline doi:10.1126/science.1085046

2. O. Hoegh-Guldberg, P. J. Mumby, A. J. Hooten, R. S. Steneck, P. Greenfield, E. Gomez, C. D. Harvell, P. F. Sale, A. J. Edwards, K. Caldeira, N. Knowlton, C. M. Eakin, R. Iglesias-Prieto, N. Muthiga, R. H. Bradbury, A. Dubi, M. E. Hatziolos, Coral reefs under rapid climate change and ocean acidification. *Science* **318**, 1737–1742 (2007). Medline doi:10.1126/science.1152509

3. C. A. Logan, J. P. Dunne, C. M. Eakin, S. D. Donner, Incorporating adaptive responses into future projections of coral bleaching. *Glob. Change Biol.* **20**, 125–139 (2014). Medline doi:10.1111/gcb.12390

4. S. R. Palumbi, D. J. Barshis, N. Traylor-Knowles, R. A. Bay, Mechanisms of reef coral resistance to future climate change. *Science* **344**, 895–898 (2014). Medline doi:10.1126/science.1251336

5. D. J. Ayre, T. P. Hughes, Genotypic diversity and gene flow in brooding and spawning corals along the Great Barrier Reef, Australia. *Evolution* **54**, 1590–1605 (2000). Medline doi:10.1111/j.0014-3820.2000.tb00704.x

6. M. J. H. Van Oppen, L. M. Peplow, S. Kininmonth, R. Berkelmans, Historical and contemporary factors shape the population genetic structure of the broadcast spawning coral, *Acropora millepora*, on the Great Barrier Reef. *Mol. Ecol.* **20**, 4899–4914 (2011). Medline doi:10.1111/j.1365-294X.2011.05328.x

7. P. K. Ingvarsson, Restoration of genetic variation lost - the genetic rescue hypothesis. *Trends Ecol. Evol.* **16**, 62–63 (2001). Medline doi:10.1016/S0169-5347(00)02065-6

8. E. Meyer, G. V. Aglyamova, M. V. Matz, Profiling gene expression responses of coral larvae (*Acropora millepora*) to elevated temperature and settlement inducers using a novel RNA-Seq procedure. *Mol. Ecol.* **20**, 3599–3616 (2011). Medline

9. D. J. Barshis, J. T. Ladner, T. A. Oliver, F. O. Seneca, N. Traylor-Knowles, S. R. Palumbi, Genomic basis for coral resilience to climate change. *Proc. Natl. Acad. Sci. U.S.A.* **110**, 1387–1392 (2013). Medline doi:10.1073/pnas.1210224110

10. R. L. Tatusov, N. D. Fedorova, J. D. Jackson, A. R. Jacobs, B. Kiryutin, E. V. Koonin, D. M. Krylov, R. Mazumder, S. L. Mekhedov, A. N. Nikolskaya, B. S. Rao, S. Smirnov, A. V. Sverdlov, S. Vasudevan, Y. I. Wolf, J. J. Yin, D. A. Natale, The COG database: An updated version includes eukaryotes. *BMC Bioinformatics* **4**, 41 (2003). Medline doi:10.1186/1471-2105-4-41

11. P. Langfelder, S. Horvath, WGCNA: An R package for weighted correlation network analysis. *BMC Bioinformatics* **9**, 559 (2008). Medline doi:10.1186/1471-2105-9-559

12. S. Wang, E. Meyer, J. K. McKay, M. V. Matz, 2b-RAD: A simple and flexible method for genome-wide genotyping. *Nat. Methods* **9**, 808–810 (2012). Medline doi:10.1038/nmeth.2023

13. L. A. Hoekstra, M. A. Siddiq, K. L. Montooth, Pleiotropic effects of a mitochondrial-nuclear incompatibility depend upon the accelerating effect of temperature in *Drosophila*. *Genetics* **195**, 1129–1139 (2013). Medline doi:10.1534/genetics.113.154914

14. O. Hoegh-Guldberg, L. Hughes, S. McIntyre, D. B. Lindenmayer, C. Parmesan, H. P. Possingham, C. D. Thomas, Ecology. Assisted colonization and rapid climate change. *Science* **321**, 345–346 (2008). Medline doi:10.1126/science.1157897

15. E. Meyer, S. Davies, S. Wang, B. L. Willis, D. Abrego, T. E. Juenger, M. V. Matz, Genetic variation in responses to a settlement cue and elevated temperature in the reef-building coral *Acropora millepora*. *Mar. Ecol. Prog. Ser.* **392**, 81–92 (2009). doi:10.3354/meps08208

16. J. D. Hadfield, MCMC methods for multi-response generalized linear mixed models: The MCMCglmm R package. *J. Stat. Softw.* **33**, 1–22 (2010).

17. A. Moya, L. Huisman, E. E. Ball, D. C. Hayward, L. C. Grasso, C. M. Chua, H. N. Woo, J. P. Gattuso, S. Forêt, D. J. Miller, Whole transcriptome analysis of the coral *Acropora millepora* reveals complex responses to CO_2-driven acidification during the initiation of calcification. *Mol. Ecol.* **21**, 2440–2454 (2012). Medline doi:10.1111/j.1365-294X.2012.05554.x

18. R. Bourgon, R. Gentleman, W. Huber, Independent filtering increases detection power for high-throughput experiments. *Proc. Natl. Acad. Sci. U.S.A.* **107**, 9546–9551 (2010). Medline doi:10.1073/pnas.0914005107

19. W. C. Dunlap, A. Starcevic, D. Baranasic, J. Diminic, J. Zucko, R. Gacesa, M. J. van Oppen, D. Hranueli, J. Cullum, P. F. Long, KEGG orthology-based annotation of the predicted proteome of *Acropora digitifera*: ZoophyteBase - an open access and searchable database of a coral genome. *BMC Genomics* **14**, 509 (2013). 10.1186/1471-2164-14-509 Medline doi:10.1186/1471-2164-14-509

20. S. F. Altschul, T. L. Madden, A. A. Schäffer, J. Zhang, Z. Zhang, W. Miller, D. J. Lipman, Gapped BLAST and PSI-BLAST: A new generation of protein database search programs. *Nucleic Acids Res.* **25**, 3389–3402 (1997). Medline doi:10.1093/nar/25.17.3389

21. R. Nielsen, C. Bustamante, A. G. Clark, S. Glanowski, T. B. Sackton, M. J. Hubisz, A. Fledel-Alon, D. M. Tanenbaum, D. Civello, T. J. White, J. J Sninsky, M. D. Adams, M. Cargill, A scan for positively selected genes in the genomes of humans and chimpanzees. *PLOS Biol.* **3**, e170 (2005). Medline doi:10.1371/journal.pbio.0030170

22. C. Kosiol, T. Vinar, R. R. da Fonseca, M. J. Hubisz, C. D. Bustamante, R. Nielsen, A. Siepel, Patterns of positive selection in six mammalian genomes. *PLOS Genet.* **4**, e1000144 (2008). Medline doi:10.1371/journal.pgen.1000144

23. C. R. Voolstra, S. Sunagawa, M. V. Matz, T. Bayer, M. Aranda, E. Buschiazzo, M. K. Desalvo, E. Lindquist, A. M. Szmant, M. A. Coffroth, M. Medina, Rapid evolution of coral proteins responsible for interaction with the environment. *PLOS ONE* **6**, e20392 (2011). Medline doi:10.1371/journal.pone.0020392

24. S. W. Davies, M. Rahman, E. Meyer, E. A. Green, E. Buschiazzo, M. Medina, M. V. Matz, Novel polymorphic microsatellite markers for population genetics of the endangered Caribbean star coral, *Montastraea faveolata*. *Mar. Biodivers.* **43**, 167–172 (2013). doi:10.1007/s12526-012-0133-4

25. A. McKenna, M. Hanna, E. Banks, A. Sivachenko, K. Cibulskis, A. Kernytsky, K. Garimella, D. Altshuler, S. Gabriel, M. Daly, M. A. DePristo, The Genome Analysis Toolkit: A MapReduce framework for analyzing next-generation DNA sequencing data. *Genome Res.* **20**, 1297–1303 (2010). Medline doi:10.1101/gr.107524.110

26. M. A. DePristo, E. Banks, R. Poplin, K. V. Garimella, J. R. Maguire, C. Hartl, A. A. Philippakis, G. del Angel, M. A. Rivas, M. Hanna, A. McKenna, T. J. Fennell, A. M. Kernytsky, A. Y. Sivachenko, K. Cibulskis, S. B. Gabriel, D. Altshuler, M. J. Daly, A framework for variation discovery and genotyping using next-generation DNA sequencing data. *Nat. Genet.* **43**, 491–498 (2011). Medline doi:10.1038/ng.806

27. B. Langmead, S. L. Salzberg, Fast gapped-read alignment with Bowtie 2. *Nat. Methods* **9**, 357–359 (2012). Medline doi:10.1038/nmeth.1923

28. P. Danecek, A. Auton, G. Abecasis, C. A. Albers, E. Banks, M. A. DePristo, R. E. Handsaker, G. Lunter, G. T. Marth, S. T. Sherry, G. McVean, R. Durbin, 1000 Genomes Project Analysis Group, The variant call format and VCFtools. *Bioinformatics* **27**, 2156–2158 (2011). Medline doi:10.1093/bioinformatics/btr330

29. P. Stam, Construction of integrated genetic linkage maps by means of a new computer package : JOINMAP. *Plant J.* **3**, 739–744 (1993). doi:10.1111/j.1365-313X.1993.00739.x

30. J. W. van Ooijen, JoinMap 4 (2006).

31. J. C. Kenyon, Models of reticulate evolution in the coral genus *Acropora* based on chromosome numbers: Parallels with plants. *Evolution* **51**, 756–767 (1997). doi:10.2307/2411152

32. R. Fisher, On the interpretation of $\chi2$ from contingency tables, and the calculation of P. *J.R. Stat. Soc.* **85**, 87–94 (1922). doi:10.2307/2340521

33. R. A. Fisher, *Statistical Methods for Research Workers* (Oliver and Boyd, Edinburgh, UK, 1932).

34. M. C. Whitlock, Combining probability from independent tests: The weighted Z-method is superior to Fisher's approach. *J. Evol. Biol.* **18**, 1368–1373 (2005). Medline doi:10.1111/j.1420-9101.2005.00917.x

35. Y. Benjamini, Y. Hochberg, Controlling the false discovery rate: A practical and powerful approach to multiple testing. *J. R. Stat. Soc. B* **57**, 289–300 (1995).

36. S. Otto, T. Day, *A Biologist's Guide to Mathematical Modeling in Ecology and Evolution* (Princeton Univ. Press, Princeton, NJ, 2007); http://press.princeton.edu/titles/8458.html.

37. D. A. Okar, A. J. Lange, Fructose-2,6-bisphosphate and control of carbohydrate metabolism in eukaryotes. *Biofactors* **10**, 1–14 (1999). Medline doi:10.1002/biof.5520100101

38. P. R. Gardner, D. D. Nguyen, C. W. White, Aconitase is a sensitive and critical target of oxygen poisoning in cultured mammalian cells and in rat lungs. *Proc. Natl. Acad. Sci. U.S.A.* **91**, 12248–12252 (1994). Medline doi:10.1073/pnas.91.25.12248

39. R. W. Frazee, W. E. Walden, E. C. Theil, Aconitase activities of FeS IRP-1 and m-aconitase: Evolution of the RNA binding properties coincide with low activity and sensitivity to degradation. *J. Inorg. Biochem.* **59**, 547 (1995). doi:10.1016/0162-0134(95)97642-4

40. S. D. Quistad, A. Stotland, K. L. Barott, C. A. Smurthwaite, B. J. Hilton, J. A. Grasis, R. Wolkowicz, F. L. Rohwer, Evolution of TNF-induced apoptosis reveals 550 My of functional conservation. *Proc. Natl. Acad. Sci. U.S.A.* **111**, 9567–9572 (2014). Medline doi:10.1073/pnas.1405912111

41. A. Verkhratsky, G. Burnstock, Biology of purinergic signalling: Its ancient evolutionary roots, its omnipresence and its multiple functional significance. *BioEssays* **36**, 697–705 (2014). Medline doi:10.1002/bies.201400024